3.RESULTS

3.1. Effect of PKC activators on the phosphorylation and localisation of occludin in MDCK cells cultivated in low calcium medium.

3.1.1 Effects of PKC activators on the TX-100 solubility and phosphorylation of occludin.

Epithelial cells maintained in a low calcium cultivation medium lose intercellular junctions, providing a suitable model for studying tight junction assembly (Martinez-Palomo et al., 1980; Sakakibara et al., 1997). As reviewed in the Introduction, the diacylglycerols, activators of PKC, are known to induce formation of TJ strands in MDCK cells despite cultivation in low calcium medium (Balda et al., 1993). The molecular pathways involved in TJs strand formation remain unclear, although the phosphorylation of as yet unidentified proteins by PKC is implicated. The transmembrane tight junction protein occludin is the only known tight junction component for which the extent of phosphorylation correlates well with the localisation to the tight junction (Sakakibara et al., 1997; Wong, 1997). It is therefore possible, that occludin is phosphorylated during diacylglycerol-induced tight junction assembly. To evaluate this possibility, we investigated the effect of PKC activators on the phosphorylation state of occludin. To assess changes in phosphorylation, MDCK cells have been placed in low calcium (LC) medium, which leads to dephosphorylation of occludin and provides suitable conditions to study the effects of PKC activators.

Previous studies have shown that TJ -localised occludin cannot be extracted from confluent epithelial cells with non-ionic detergents and shows a decreased electrophoretic mobility due to extensive phosphorylation (Sakakibara et al., 1997; Wong, 1997). In accordance with literature data (Wong, 1997), occludin extracted with TX-100-containing buffer from control MDCK cells, grown in normal calcium (NC) medium, migrated as a single band with an apparent molecular weight of about 60 kDa (Figure 3.1A, *lane 1, S*). Occludin from the TX-100 insoluble fraction migrated as multiple unresolved bands with apparent molecular weights ranging between 60 and 82 kDa (Figure 3.1A, *lane 1, I*). When MDCK cells were incubated in LC medium in order to disassemble TJs, the high molecular weight bands disappeared from the TX-100 insoluble fraction, and the amount of TX-100 insoluble occludin decreased significantly (Fig. 3.1A, *lane 2*) reflecting dephosphorylation of occludin. When TJ re-assembly was induced by switch from low to normal calcium conditions the banding pattern of TX-100 insoluble occludin was restored (Fig. 3.1A, *lane 3*). Four hours after MDCK treatment with 2 nM phorbol 12-myristate 13-acetate (PMA, a potent activator of protein kinase C) in LC medium, the

amount of TX-100 insoluble occludin increased significantly and a portion of occludin underwent an upward band shift (Fig. 3.1A, *lane 4*). The treatment of cells in LC medium with 25 nM PMA for 4 hours resulted in a further increase in the amounts of TX-100 insoluble occludin and in the degree of upward band shift, with a concomitant decrease in the amount of TX-100 soluble occludin (Fig. 3.1A, *lane 5*). An increase in TX-100 insoluble occludin and an upward band shift were also evident if MDCK cells cultivated in LC medium were treated with another PKC activator 1,2-dioctanoylglycerol (diC8) for 4 hours (Fig. 3.1A, *lane 6*).

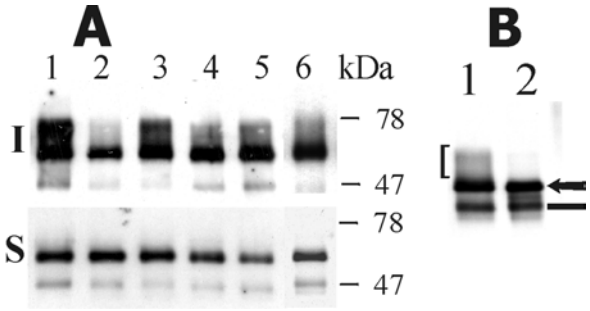

Figure 3.1 PMA and diC8 induce the phosphorylation of occludin in MDCK cells incubated in low Ca^{2+} medium. Panel A, immunoblot analysis of occludin in the TX-100-soluble (S) and –insoluble (I) fractions of MDCK-cells incubated in normal Ca^{2+} medium (lane 1) or in low Ca^{2+} medium (lane 2). MDCK cells cultivated in low-calcium medium were subjected to a calcium switch (lane 3), or treated with 2 nM (lane 4), 25 nM PMA (lane 5) or 0.5 mM diC8 (lane 6) for 4 hours. Treatment of MDCK cells cultivated in low calcium medium with PMA or diC8 induced an upward band shift of occludin.
B, immunoblot analysis of the TX-100-insoluble fraction of immunoprecipitated occludin from MDCK cells cultivated in low calcium medium and stimulated with 10 nM PMA for 20 min. Samples were either left untreated (lane 1) or subjected to the treatment with alkaline phosphatase (lane 2), resolved by electrophoresis, and then analysed by immunoblotting. Alkaline phosphatase treatment completely abolishes the upward band shift caused by PMA treatment. The arrow shows the position of non-phosphorylated occludin, the dash shows the position of antibody heavy chain, a bracket denotes the position of multiple phosphorylated forms of occludin.

The multiple occludin bands revealed by immunoblotting analysis probably represent differently phosphorylated occludin molecules. In order to show that the upward band shift of occludin induced by PMA was due to phosphorylation, MDCK cells grown in LC medium were treated with PMA and occludin immunoprecipitated from the TX-100 insoluble fraction was subjected to in vitro phosphatase treatment. Figure 3.1B shows that the additional high molecular weight occludin bands disappeared upon a treatment with alkaline phosphatase. Therefore, the upward band shift of occludin induced by PMA and diC8 is due to phosphorylation of occludin.

To characterise the occludin phosphorylation by PKC activators in greater detail, we examined the time and concentration dependence of PMA-induced changes in electrophoretic mobility of occludin (Fig. 3.2). As high molecular weight bands corresponding to phosphorylated occludin were invariably found to be insoluble in TX-100-containing buffer, only TX-100 insoluble fractions were analysed.

The addition of PMA to MDCK cells incubated in LC medium resulted in a dose-dependent phosphorylation of occludin (Fig. 3.2A). When PMA was added for 1 hour, the phosphorylation was evident at concentrations as low as 2.5 nM PMA and reached a maximum at 25 nM PMA. This maximum level of PMA-induced occludin phosphorylation is identical (within the accuracy of immunoblot technique) to the level of occludin phosphorylation in MDCK cells maintained in normal calcium conditions (Fig. 3.2A, *NC*).

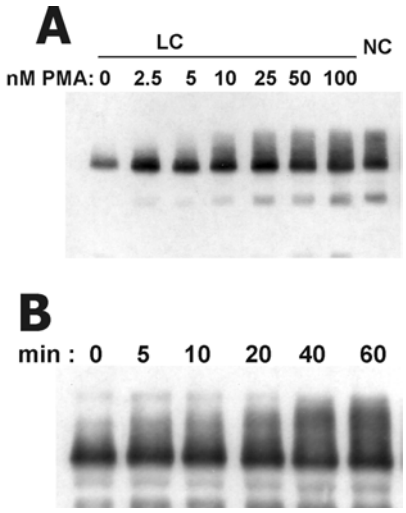

Figure 3.2 Time and concentration dependence of occludin phosphorylation in MDCK cells upon the treatment with PMA. Immunoblot analysis of occludin in the TX-100-insoluble fraction of MDCK cells. After incubation of cell monolayers in low-calcium medium for 20 hours, PMA at the indicated concentrations was added for 1 hour (A) or 25 nM PMA was added for the indicated periods of time (B).

The time dependence of occludin phosphorylation in MDCK cells induced by 25 nM PMA in LC is shown in Figure 3.2B. The upward band shift due to phosphorylation became evident after 5 min and reached a maximum 40 minutes after PMA addition.

3.1.2 Effects of PKC activators on the subcellular localisation of occludin.

Next, we verified whether the PMA/diC8-mediated increase in the phosphorylation state of occludin is accompanied by the translocation of occludin to the sites of cell-cell contacts. The cellular distribution of occludin was examined by immunofluorescence microscopy. In accordance with previous reports (Sakakibara et al., 1997) occludin was intensively stained at cell-cell contacts in confluent MDCK cells in normal Ca^{2+} medium, indicating the formation of continuous TJs (Fig. 3.3A). After incubation of MDCK cells in LC medium, occludin became localised almost exclusively in the cytoplasm, indicating a loss of TJ architecture (Fig. 3.3B). When PMA at 2 nM was added for two hours to the cells in LC medium, a portion of occludin was translocated to the plasma membrane at the regions of cell-cell contact (Fig. 3.3C, arrows). Staining of occludin at intercellular contacts was not as continuous or intensive as in the cells grown in NC (Fig. 3.7A). Prolongation of the incubation period up to 4 hours further increased

the amount of occludin translocated to regions of intercellular contact (Fig. 3.3D). When 25 nM PMA was used to stimulate cells maintained in LC-medium, occludin translocated to the periphery and showed a more discontinuous and intensive staining compared to samples treated with 2 nM PMA (Fig. 3.3E). A large portion of occludin was still localised in the cytoplasm, although cytoplasmic staining became discontinuous as judged from the appearance of large occludin-positive granular structures (Fig. 3.3E, arrowheads). Prolongating of the incubation time to 4 hours did not change the distribution pattern significantly (Fig. 3.3F), although a decrease in the amount of occludin localised at cell-cell contacts was discernible.

Treatment of MDCK cells in LC medium with diC8 (0.5 mM) resulted in redistribution of occludin, similar to the effect of 2 nM PMA. Fragmentary staining of occludin at cell-cell contacts was evident two hours after the addition of diC8 (Fig. 3.3G). With prolonged incubation time up to 4 hours, the staining of occludin at cell borders became more continuous, and the amount of occludin translocated to cell-cell contacts increased further (Fig. 3.3H).

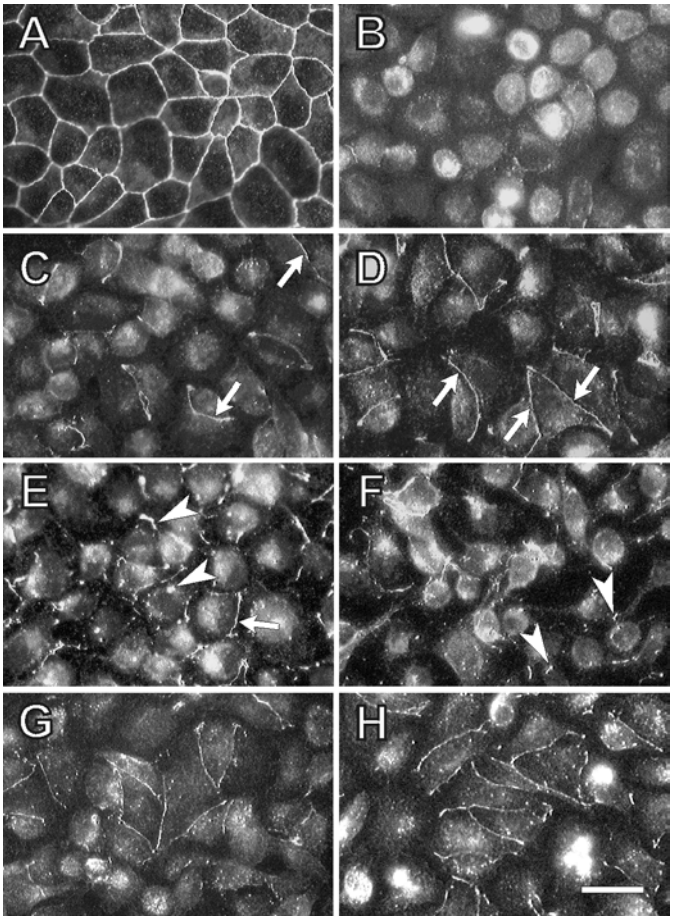

Figure 3.3 PMA and diC8 induce the translocation of occludin from the cytoplasm to the lateral cell membrane in MDCK cells incubated in low Ca^{2+} medium. MDCK cells were incubated in low-calcium medium for 20 hours after which PMA, diC8 or Ca^{2+} was added. Cells cultivated in normal calcium medium show continuous staining of occludin at cell-cell contacts (A). After cultivation of cells in low calcium medium the occludin signal was detected mainly from small granular structures in the cytoplasm (B). Two hours after the addition of 2 nM PMA staining of occludin at cell borders (arrows) was evident (C). Prolongation of the incubation period to 4 hours further increased the amount of occludin migrating to the cell borders (D). When 25 nM PMA was used to stimulate the cells for 2 hours, large granular structures were found in the cytoplasm (arrowheads) and occludin staining at the cell borders became discontinuous (E). Prolongation of the incubation period (25 nM PMA) up to 4 hours led to some decrease in the amount of occludin found at cell-cell contacts (F). Two hours after the addition of 0.5 mM diC8 staining of occludin at cell borders was evident (G). Prolongation of the incubation period to 4 hours further increased the amount of occludin at cell borders (H). Scale bar, 10 µm

3.1.3 Effects of GF-109203X on the phosphorylation and cellular redistribution of occludin induced by PKC activators.

Besides PKC, phorbol esters and DAG may activate a number of other proteins in mammalian cells (see Introduction). In order to functionally separate PKC-specific effects from those mediated by alternative DAG/phorbol-ester receptors, we applied GF-109203X – a PKC-specific inhibitor. GF-109203X effectively competes for the ATP-binding site of conventional and novel PKCs, and while the IC_{50} of the compound is in low nanomolar range against cPKC and 200-700 nM against different nPKC it shows much lower efficiency against atypical PKC with a IC_{50} of approximately 5.8 μM for PKCζ (Toullec *et al.*, 1991; Martiny-Baron *et al.*, 1993).

To investigate the involvement of PKC in the regulation of occludin targeting to cell-cell contact sites, the assembly of TJs was induced by the addition of PMA or diC8 to MDCK cells maintained in LC medium in the presence or absence of GF-109203X. Occludin localisation was assessed by immunofluorescence microscopy. Four hours after the addition of PKC activators, fragmentary occludin staining was evident at intercellular contacts, indicating the recruitment of occludin into tight junctions (Fig. 3.5A, *PMA* and Fig. 3.5A, *diC8*). Inhibition of PKC with 5 μM GF-109203X resulted in a very weak staining of occludin at the intercellular contacts and in a prominent staining in cytoplasm (Fig. 3.5A, *PMA+GF* and Fig. 3.5A, *diC8+GF*). These data indicate that PKC mediates the effects of PMA and diC8 on cellular redistribution of occludin under LC conditions.

To further test the hypothesis that PKC is involved in occludin phosphorylation, the effect of GF-109203X on PMA/diC8-induced occludin phosphorylation was investigated. The characteristic multiple-band pattern of phospho-occludin was seen on immunoblot of TX-100 insoluble fractions of MDCK cells maintained in NC medium (Fig. 3.4B, *NC*). High molecular weight bands disappeared when cells were incubated in LC medium, indicating the dephosphorylation of occludin (Fig. 3.4, *LC*). Four hours after the addition of 2.5 nM PMA or 0.5 mM diC8, a profound upward band shift of occludin was visible on immunoblot, reflecting the increased phosphorylation of occludin (Fig. 3.4, *+PMA*, *+diC8*). Pan-PKC inhibitor GF-109203X at 5 μM markedly decreased upward band shift, indicating that the occludin phosphorylation under stimulation by PMA/diC8 in LC conditions is mediated by protein kinase C.

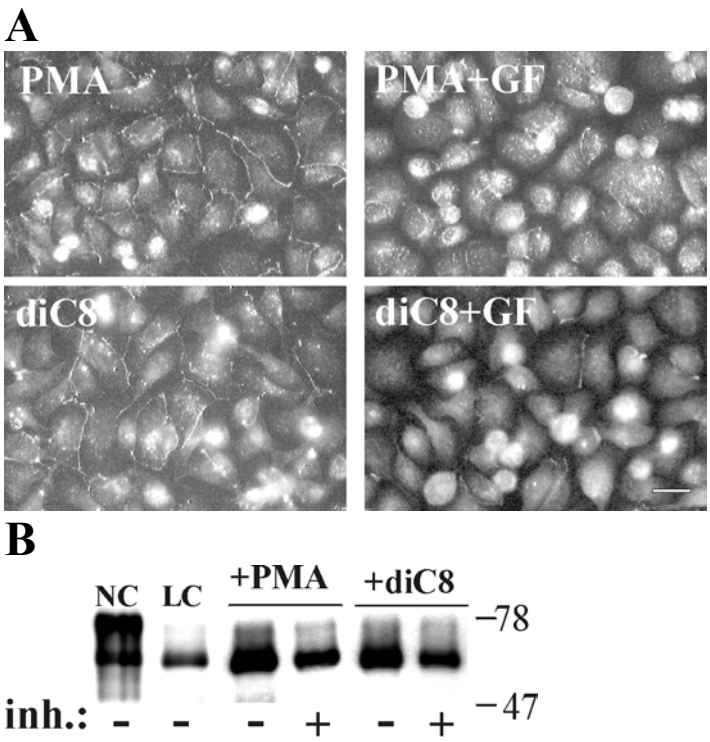

Fig. 3.4 PKC inhibitor GF-109203X decreases both the phosphorylation and re-distribution of occludin induced by PKC activators.
Panel A, 2.5 nM PMA or 0.5 mM diC8 were added to the cells cultivated in LC-medium with or without 5 μM GF-109203X (GF). Figure shows immunofluorescent localisation of occludin 4 h after addition of PMA or diC8. Scale bar, 10 μm.
B, Figure shows immunoblot analysis of occludin in Triton X-100 insoluble fractions of MDCK cells. Cells were harvested after cultivation in NC- or in LC-medium (NC and LC). In addition, 2.5 nM PMA or 0.5 mM diC8 were added to the cells cultivated in LC-medium with or without 5 μM GF-109203X (inh.).

3.2. Effects of PKC inhibitors on phosphorylation and redistribution of occludin induced by Ca^{2+} Switch.

3.2.1 Effects of GF-109203X and Gö6976.

Taking into account that activation of PKC by PMA and diC8 triggers occludin phosphorylation and translocation to the plasma membrane under LC conditions, we suggest that PKC may be a physiological regulator of occludin function. To collect more evidence on the functional regulation of occludin by PKC, we investigated the effects of PKC inhibitors on the phosphorylation and incorporation of occludin into newly assembling tight junctions. In these experiments, assembly of cell junctional complexes has been initiated by the switch to NC medium in the presence or absence of PKC inhibitors, and cellular distribution and phosphorylation of occludin has been monitored as described above.

In normal calcium conditions, occludin localises at cell junctional complex (Figure 3.5A, *NC*) and the TX-100 insoluble fraction of occludin is highly phosphorylated (Figure 3.5B, *NC*). Overnight incubation of MDCK cells in low calcium medium disrupts TJs, as evidenced by the decreased phosphorylation state and exclusively cytoplasmic staining of occludin (Figs. 3.5A, and 3.5B, *LC*). Four hours after the switch to NC medium, TJ development is obvious from the increased phosphorylation state (Fig. 3.5B, $+Ca^{2+}$) and a prominent staining of occludin at cell-cell contacts (Figs. 3.5A, $+Ca^{2+}$). The significant cytoplasmic staining of occludin along with

occasional gaps in staining at the cell border indicates that TJ assembly is not yet complete at 4 hours time point (*cf*. Fig. 3.5A, *NC* and Fig. 3.5A $+Ca^{2+}$). Both the upward shift of occludin and re-distribution of occludin to cell borders caused by calcium switch were significantly blocked by 5 μM of pan-PKC inhibitor GF-109203X (Figs. 3.5A and 3.5B, $+Ca^{2+}$+*GF*). These data strongly suggest that the signaling by PKC is required for calcium switch-induced occludin phosphorylation and tight junction assembly.

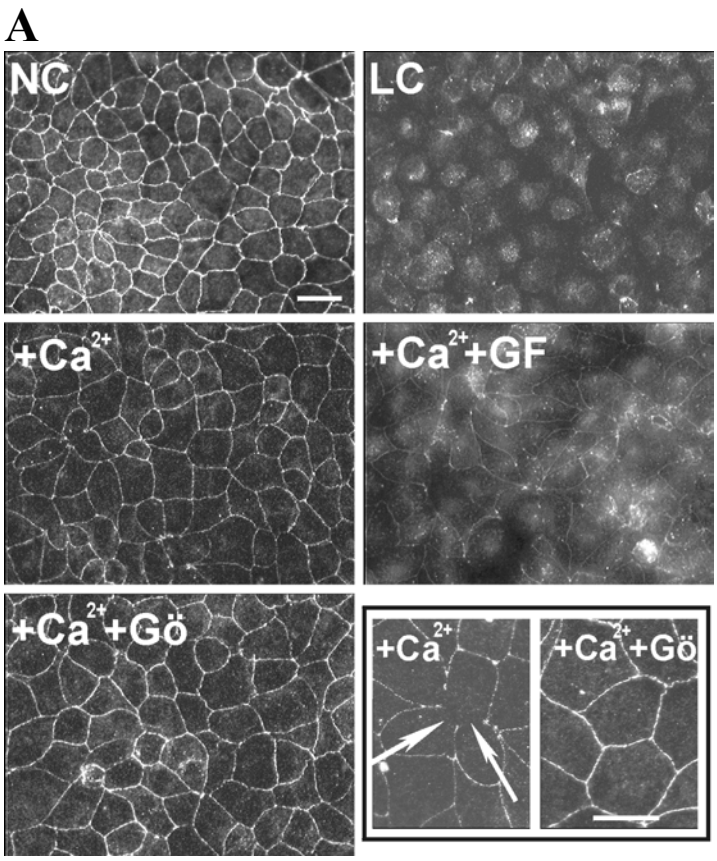

Figure 3.5 The effect of GF-109203X and Gö6976 on tight junction assembly and occludin phosphorylation induced by calcium switch. Panel A, MDCK cells cultivated in normal calcium medium (NC) show continuous staining of occludin at cell-cell contacts. After cultivation of cells in low calcium medium (LC) the occludin signal was detected mainly in the cytoplasm. Four hours after the addition of NC medium to the cells which were cultivated in LC medium incorporation of occludin into forming tight junction is evident ($+Ca^{2+}$).
The presence of 5 μM of pan-PKC inhibitor GF-109203X suppressed occludin incorporation into newly forming tight junctions ($+Ca^{2+}$, +GF). Conventional PKC inhibitor Gö6976 (5 μM) did not inhibit occludin redistribution ($+Ca^{2+}$, +Gö). Furthermore, examination of the images at higher magnification (framed) revealed that occludin staining is weaker and more discontinuous (arrows) in the absence of Gö6976. Scale bars, 20 μM
B, immunoblot analysis of occludin. High molecular weight bands of occludin in normal calcium (NC) conditions disappear in low calcium (LC). Four hours after switch to normal calcium upward band shift due to phosphorylation is observed ($+Ca^{2}$, 4 h) which is reduced by 5 μM GF109203X (+GF) but not by 5 Gö6976 (+Gö).

Since GF-109203X inhibits conventional and novel PKC isozymes and, to a much lower extent, atypical PKCs (Martiny-Baron et al., 1993), no conclusion can be reached on the involvement of particular subfamilies of PKC isozymes in tight junction formation. In order to functionally separate the contribution of conventional PKC (cPKC) from the contribution of

other PKC family members, we studied the effects of small molecule inhibitor Gö6976. Gö6976 potently and selectively inhibits cPKC isozymes and PKCμ/PKD, with no effect on novel or atypical PKCs even at micromolar concentrations (Martiny-Baron et al., 1993; Gschwendt et al., 1996).

Significantly, Gö6976 at 5 μM inhibited neither occludin phosphorylation nor its redistribution to cell borders (Figs. 3.5A and 3.5B, $+Ca^{2+}+Gö$). Furthermore, closer examination revealed that occludin staining at intercellular contacts is even more prominent and continuous in MDCK cells treated with Gö6976 as compared to untreated cells (note occassinal dicontinuities in occludin staining (arrows) and weaker occludin signal at cell borders in the absence of Gö6976 shown on framed images of Fig. 3.5A). These data clearly indicate that signalling by conventional PKC is not required for TJ assembly, indicating that nPKC and aPKC subfamilies may be positive regulators of tight junction assembly.

3.2.2 Gö6976 promotes occludin phosphorylation and tight junction formation.

The data obtained imply that the inhibition of conventional PKC with Gö6976 does not block TJ assembly. Rather, Gö6976 seems to support tight junction assembly as evidenced by accelerated incorporation of occludin into assembling tight junction (framed images on Fig. 3.5A). No effect of Gö6976 on occludin phosphorylation has been observed; however, since occludin phosphorylation precedes its incorporation into the TJ, the effects of Gö6976 on occludin phosphorylation would be observed at earlier stages of TJ assembly. To examine whether Gö6976 would accelerate the phosphorylation of occludin, we examined the time-course of occludin phosphorylation in MDCK following the switch to NC from LC medium in the presence and the absence of Gö6976. The time course of occludin phosphorylation during tight junction assembly induced by the calcium switch is shown on Fig. 3.6A. In the absence of Gö6976, the upward band shift due to phosphorylation is negligible after 20 min, first becomes evident after 40 min, reaching a maximum after about 3 hours (Fig. 3.6A, $+Ca^{2+}$). The presence of Gö6976 at 5 μM strongly promotes occludin phosphorylation during calcium switch with higher molecular weight occludin bands appearing already after 20 min and the most prominent effect being observed 60 min after the switch to NC medium (Fig. 3.6A, $+Ca^{2+}+ Gö$).

The dose dependence of occludin phosphorylation on Gö6976 is shown in Figure 3.6B. In this experiment, Gö6976 was added at different concentrations along with normal calcium medium to the cells previously maintained in LC. When cells were analysed 40 min after

switching to NC medium, upward band shift of occludin was evident at 80 nM of Gö6976, reaching a maximum at 600 nM of Gö6976.

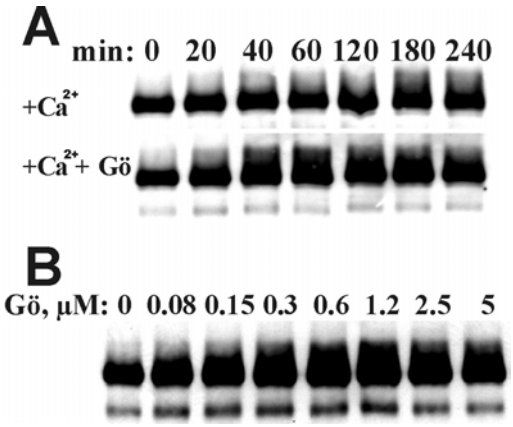

Figure 3.6 Go6976 dose-dependently accelerates the phosphorylation of occludin during calcium switch. Immunoblot analysis of occludin in the TX-100-insoluble fractions of MDCK-cells cultivated in low-calcium medium and subjected to a calcium switch. Panel A, switch was performed in the absence ($+Ca^{2+}$) or in the presence of 5 µM of Gö6976 ($+Ca^{2+}$, +Gö). Samples were collected at indicated time. The calcium switch caused gradual upward band shift of occludin due to phophosphorylation reaching a maximum at about 3 h. In the presence of Gö6976 the phosphorylation proceeded much faster reaching a maximum at about 40 min.
B, calcium switch was performed in the presence of Gö6976 at indicated concentrations. Gö6976 affects occludin phosphorylation dose-dependently, reaching a maximum at about 600 nM.

Immunofluorescent staining revealed that Gö6976 accelerated the redistribution of occludin from cytoplasm to the sites of cell-cell contact. As shown in Figure 3.7, 40 minutes after switch to NC medium the presence of occludin is evident at relatively few intercellular contacts (Fig. 3.7, no Gö), whereas more prominent and continuous staining of occludin at most cell-cell contacts is observed in the presence of Gö6976 at 150 nM (Fig. 3.7, *+150 nM Gö*). This effect of Gö6976 also seems to be dose-dependent, since the increase in the concentration of Gö6976 to 1 µM resulted in the further increase of occludin signal at intercellular contacts (Fig. 3.7, *+1 µM Gö*). Cells treated with 5 µM of Gö6976 show continuous staining of occludin at all intercellular contacts (Fig. 3.7, *+5 µM Gö*), although occludin signal was also detected

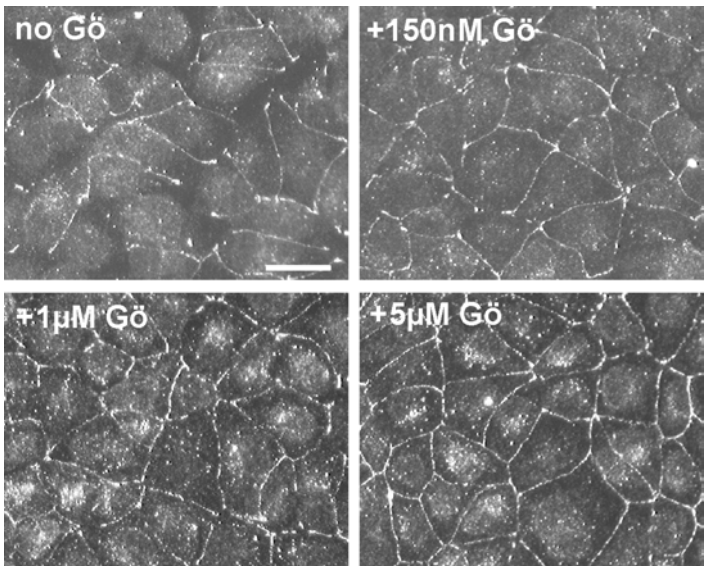

Figure 3.7 Gö6976 accelerates the incorporation of occludin into tight junction during calcium switch. Immunofluorescent localisation of occludin 40 min after the addition of calcium to MDCK cells placed in low calcium medium (no Gö). Gö6976 at 0.15, 1 and 5 µM was added to evaluate the involvement of conventional PKC in the redistribution of occludin. Scale bar, 20 µm

from large granules in cytoplasm that are normally not present in cells with completely formed TJs.

Additionally, the immunofluorescence staining revealed that the presence of Gö6976during calcium switch accelerated the incorporation of other tight junction proteins ZO-1 and claudin-1 into newly forming tight junctions (results not shown). Taken together, these data demonstrate that the inhibition of conventional PKC with Gö6976 promotes the assembly of whole tight junctional complex in MDCK cells upon switch to normal calcium conditions.

3.2.3 Rottlerin blocks the tight junction assembly and occludin phosphorylation induced by calcium switch.

The data above indicate that in contrast to pan-PKC inhibitor GF-109203X, Gö6976, the inhibitor of conventional PKC, does not block tight junction assembly, suggesting that enzyme activities of novel and/or atypical PKC isoforms are essential for tight junction assembly. To obtain more information about PKC isoforms involved in the regulation of tight junction, we studied the effect of kinase inhibitor rottlerin in a series of experiments similar to those described above for GF-109203X and Gö6976. Rottlerin is known to be active against PKCθ and -δ and inefficient against PKCε and -η, thus allowing the selective inhibition of two of four novel PKC isoforms (Gschwendt et al., 1994; Villalba et al., 1999).

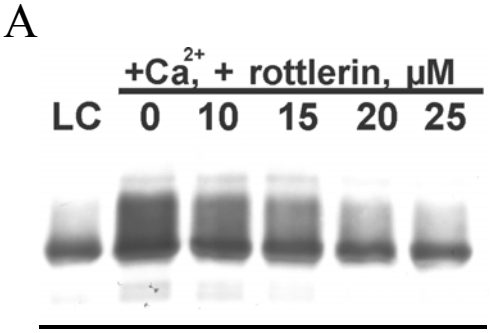

Figure 3.8 Rottlerin dose-dependently inhibits occludin phosphorylation and redistribution induced by calcium switch. MDCK cells were cultivated in low-calcium medium and subjected to the calcium switch (4 h) either in the absence or in the presence of rottlerin. A, Immunoblot analysis of occludin in the TX-100-insoluble fractions of MDCK-cells.
B, Immunofluorescent localisation of occludin after the switch to normal calcium medium without (a) or with rottlerin at 10 (b) and 15 (c) µM. Scale bar, 20 µm.

Figure 3.8 A shows that rottlerin dose-dependently inhibits the phosphorylation of occludin following the switch from low to normal calcium medium. The moderate inhibition of phosphorylation was observed at 10 μM which is typical concentration of rottlerin required for marked intracellular inhibition of PKCθ/δ (Tan et al., 2003). Full inhibition of occludin phosphorylation has been observed at 25 μM. In order to study the involvement of PKCθ/δ in the regulation of occludin targeting to cell-cell contacts, calcium switch was performed in the presence of rottlerin and occludin redistribution was analysed by immunofluorescent staining. When compared to control showing continuous staining of occludin in newly forming TJ 4 hours after switch to NC medium (Fig. 3.8B, a), the redistribution of occludin to cell contacts was strongly inhibited with 10 μM rottlerin as judged from the prominent cytoplasmic staining of occludin and marked decrease in staining intensity at intercellular contacts (Fig. 3.8B, b).

The nearly complete inhibition of occludin redistribution was achieved with 15 μM rottlerin (Fig. 3.8B, c). Furthermore, rottlerin inhibited the redistribution of another TJ protein ZO-1 in a similar concentration-dependent manner. As shown in Fig. 3.9, in untreated control monolayers od MDCK cells ZO-1 had appropriately sorted to the intercellular contacts 4 hours after Ca^{2+} switch. No cytoplasmic staining of ZO-1 could be detected at this time point (Fig. 3.9. A). Rottlerin at 10 μM resulted in obvious defects in ZO-1 sorting into newly forming TJs (Fig. 3.9. B). Interestingly, inhibitory effects of rottlerin at 10 μM were different for ZO-1 and occludin: occludin was weakly and continuously stained at nearly all cell borders and in cytoplasm (Fig. 3.8A, b), whereas ZO-1 was intensively stained at most cell borders, yet being completely absent at some intercellular contacts (Fig. 3.9. B). The application of rottlerin at 20 μM resulted in the marked retention of ZO-1 in the cytoplasm and nearly abolished its translocation to the plasma membrane (Fig. 3.9 C).

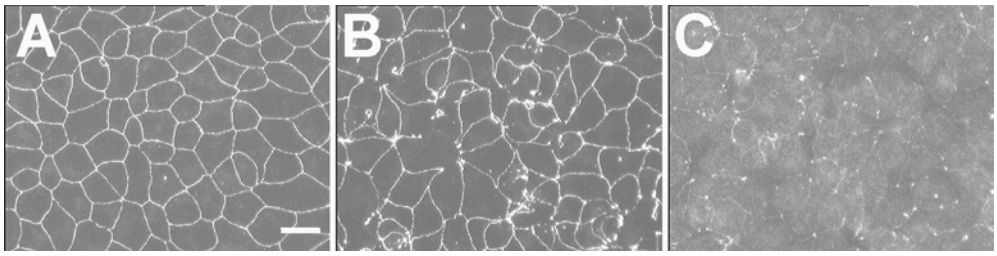

Figure 3.9 Rottlerin blocks calcium switch-induced ZO-1 redistribution to intercellular contacts. Immunostaining of ZO-1 in MDCK cells 4 hours after the calcium switch in the absence (A) or in the presence of 10 (B) and 20 (C) μM of rottlerin in normal calcium medium. Scale bar, 20 μm

Cell-permeable myristoylated pseudosubstrate inhibitor of PKCθ had no effect on occludin and ZO-1 redistribution following the addition of calcium (data not shown). It is, therefore, likely that of two kinases known to be inhibited by rottlerin, only PKCδ is involved in the control of occludin phosphorylation and TJ assembly induced by switch to normal calcium medium.

3.3 Gö6976 promotes TJ assembly induced by diC8 in LC medium.

The data above indicate that the inhibition of conventional PKC and/or PKD by Gö6976 accelerates occludin phosphorylation and TJ formation induced by calcium switch. As a next step to characterise the involvement of cPKC in tight junction assembly, we applied activators of PKC to MDCK cells maintained in LC conditions to induce fragmentary tight junctions, similarly to the experiments described in Part 3.1. The effects of Gö6976 on the redistribution of ZO-1 have been studied to evaluate the involvement of cPKC in the sorting of ZO-1 to intercellular contacts. In addition, we addressed two other important questions: (i) whether GF-109203X inhibits the formation of entire TJ complex e.g. if the inhibition of redistribution of TJ proteins other than occludin can be achieved with GF-109203X (ii) whether observed effects of GF-109203X (Figs. 3.4 and 3.5) can be attributed entirely to the inhibition of PKC.

MDCK cells cultivated in LC medium showed only very occasional ZO-1 staining at intercellular contacts (Fig.3. 12 *LC*). In agreement with previously published data (Balda et al., 1993), 4 hours after the addition of 0.5 mM diC8 a portion of ZO-1 was translocated from the cytoplasm to the sites of cell-cell contacts (Fig. 3.12 *+diC8*), reflecting a formation of fragmentary TJs at this time point. The treatment of cells with pan-PKC inhibitors GF-109203X (5 μM) or myristoylated protein kinase C inhibitor (MPKCI, 10 μM) abolished the diC8-induced redistribution of ZO-1 (Fig. 3.12 *+diC8+GF; +diC8+ MPKCI*). Thus, GF-109203X inhibits the redistribution of both occludin (Fig. 3.4) and ZO-1, suggesting that the formation of entire TJ complex is blocked by the inhibition of PKC. The inhibitory effect of structurally unrelated peptide inhibitor substantiates the importance of PKC in tight junction assembly induced by diacylglycerols, and excludes the possibility that the observed effects of GF-109203X (Figs. 3.4, 3.5 and 3.10) were due to the inhibition of a kinase other than PKC.

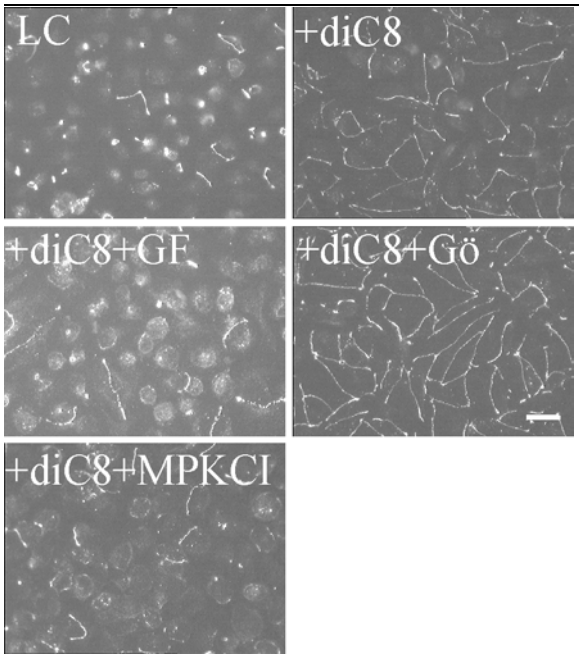

Fig. 3.10 Gö6976 promotes the incorporation of ZO-1 into tight junction induced by PKC activators. MDCK cells were placed in LC medium for 20 hours (LC), and then treated with 0.5 mM diC8 (+diC8) alone or in the presence of 5 μM GF109203X (+diC8+GF), 5 μM Gö6976 (+diC8+Gö) or 10 μM MPKCI (+diC8+MPKCI) for 4 hours. ZO-1 was visualised by indirect immuno-fluorescence staining. Scale bar, 20 μm

To investigate the involvement of cPKC subfamily in the tight junction assembly inducued by diacylglycerols in LC conditions, we used Gö6976 to selectively inhibit these isozymes. In contrast to MPKCI and GF-109203X, Gö6976 at 5 μM increased the amount of ZO-1 translocated to the plasma membrane at regions of cell-cell contact (Fig. 3.10, *+diC8 +Gö*). The staining of ZO-1 was more continuous and intensive as compared to samples treated with diC8 alone. In parallel experiments Gö6976 had similar effects on occludin and claudin-1 redistribution induced by the treatment of MDCK cells with diC8 (data not shown), indicating that not only the inhibition of cPKC failed to block the formation of TJ complex, but it also promoted the formation of tight junction.

It has been reported previously, that at the initial stage of junctional complex assembly E-cadherin and ZO-1 are precisely co-localised in areas of cell-cell contacts (Yonemura et al., 1995). Furthermore, several studies proved that intercellular adhesion of transmembrane cadherin molecules is a prerequisite for the formation of TJs (Gumbiner *et al.*, 1988; Fleming *et al.*, 1989). If effects of Gö6976 on tight junctions are cadherin-mediated, then the increase in redistribution of ZO-1 to intercellular contacts should be paralleled by the increase in accumulation of cadherins at cell-cell contact sites. To test this hypothesis we analysed cadherin distribution after the application of 0.5 mM diC8 in the presence or absence of 5 μM Gö6976. As reported before (Balda et al., 1993), in LC medium only diffuse cytoplasmic cadherin staining was observed, indicating the complete disruption of adherence junctions.

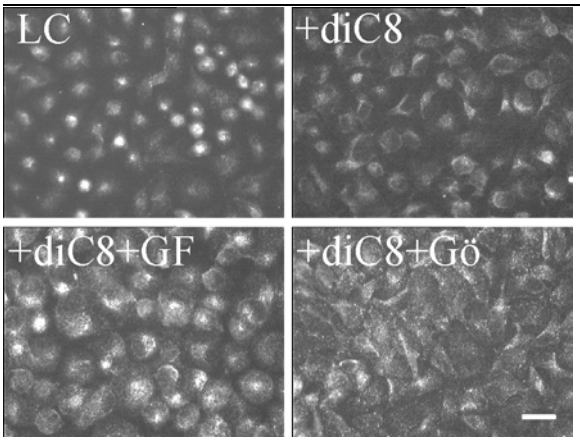

Fig.3.11 diC8 and Gö6976 do not induce redistribution of cadherins. MDCK cells were placed in LC medium for 20 hours (LC), and then treated with 0.5 mM diC8 (+diC8) alone or in the presence of 5 μM GF109203X (+diC8+GF) or 5 μM Gö6976 (+diC8+Gö) for 4 hours. Cadherins were visualised by the indirect immunofluorescence staining with anti-pan-cadherin antibodies. Scale bar, 20 μm

No lateral plasma membrane staining by anti-pan-cadherin antibodies was detected in cells treated with diC8 in LC conditions. If diC8 was added together with 5 μM Gö6976, a slight redistribution of cadherins to the cell periphery was evident, but no staining at intercellular contacts has been observed. Thus, Gö6976 promotes redistribution of TJ proteins without an obvious accumulation of cadherins at the lateral plasma membrane of diC8-stimulated MDCK cells.

3.4. Gö6976 Triggers Tight Junction Formation in MDCK Cells maintained in LC medium.

3.4.1 Effects of Gö6976 on occludin phosphorylation and distribution in LC medium.

The striking difference between the effects of GF-109203X and Gö6976 suggests that Gö6976 blocks a kinase-regulated pathway which either promotes the disassembly of tight junction or delays assembly of TJ induced by calcium switch or diacylglycerols. To further characterise the effects of Gö6976 on the assembly of tight junction we tested whether Gö6976 will trigger the formation of TJs in LC conditions similarly to diacylglycerols. Figure 3.12A shows that the addition of Gö6976 (150 nM) to MDCK cells in LC medium results in the partial redistribution of occludin to the sites of cell-cell contact. The increase in the concentration of inhibitor to 5 μM correlated with an additional increase in the amount of occludin translocated to regions of cell-cell contact (Fig. 3.12A). The redistribution of occludin was paralleled by increased phosphorylation. As shown in Figure 3.11B, the upward band shift of occludin due to phosphorylation was obvious in MDCK cells cultivated in LC medium and treated with 150 nM of Gö6976. This effect was not significantly enhanced when the concentration of Gö6976 was

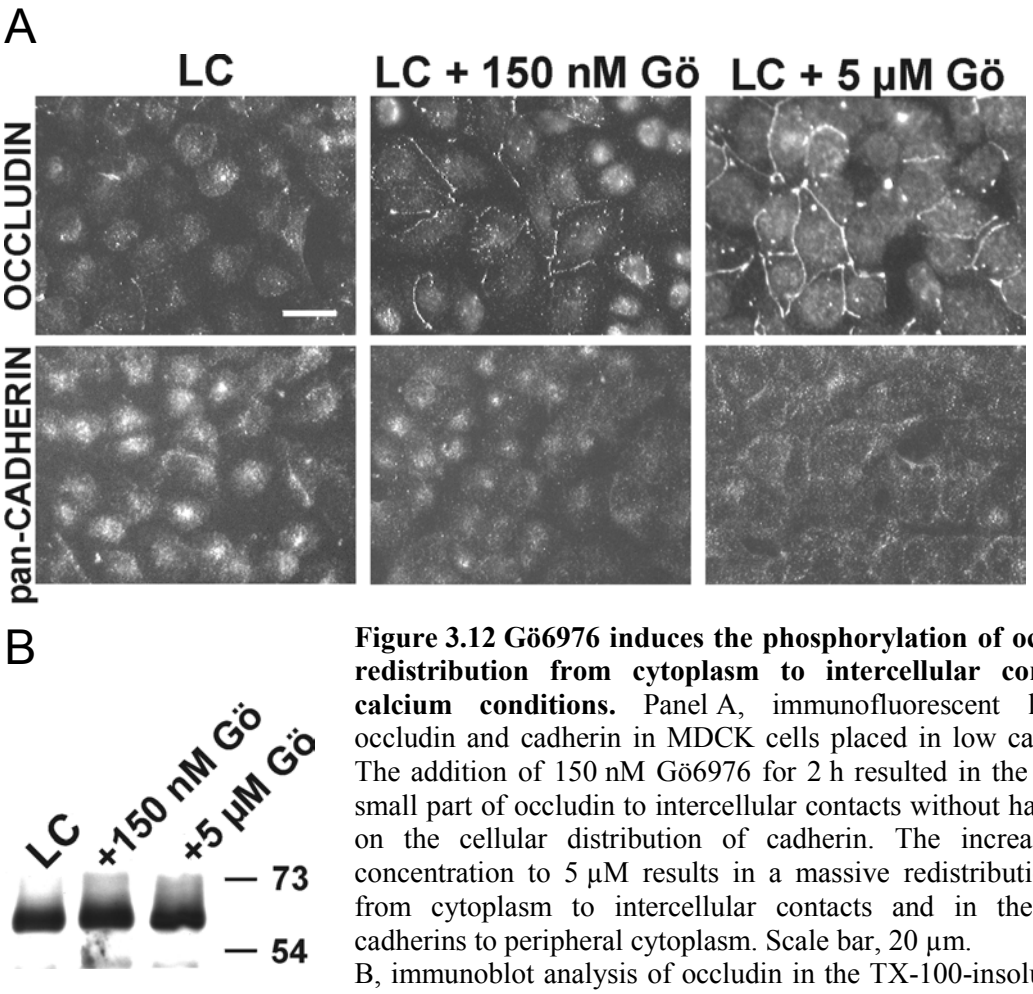

Figure 3.12 Gö6976 induces the phosphorylation of occludin and its redistribution from cytoplasm to intercellular contacts in low calcium conditions. Panel A, immunofluorescent localisation of occludin and cadherin in MDCK cells placed in low calcium medium. The addition of 150 nM Gö6976 for 2 h resulted in the relocation of a small part of occludin to intercellular contacts without having any effect on the cellular distribution of cadherin. The increase in Gö6976 concentration to 5 µM results in a massive redistribution of occludin from cytoplasm to intercellular contacts and in the relocation of cadherins to peripheral cytoplasm. Scale bar, 20 µm.
B, immunoblot analysis of occludin in the TX-100-insoluble fraction of MDCK cells cultivated in low-calcium medium (LC). The addition of 150 nM Gö6976 for 2 h resulted in upward band shift of occludin due to phosphorylation, the increase in Gö6976 concentration to 5 µM did not potentiate this effect.

increased to 5 µM. Notably, in parallel experiments Gö6976 did not induce the redistribution of cadherins to the junction complex in low calcium medium (Fig. 3.12A). The only notable changes in the distribution of cadherins were evident at 5 µM of Gö6976; cadherins moved from central areas of cells to peripheral cytoplasm (Fig. 3.12A).

3.4.2 Gö6976 Triggers the Formation of Tight Junction Complexes in LC Medium.

The effects of Gö6976 on occludin redistribution and phosphorylation suggest that Gö6976 triggers the redistribution of occludin to intercellular contacts in low calcium conditions which is independent from cadherin-mediated cell-cell adhesion. However, it is not clear to what extent the Gö6976-mediated redistribution of occludin to sites of cell-cell contact reflects the more general formation of tight junctions. To address this question we explored the effects of Gö6976 on the cellular distribution of other tight junction proteins ZO-1, ZO-2 and claudin-1.

These proteins were well localised to the cell junction of confluent MDCK cells in normal Ca^{2+} medium (Fig. 3.13A, *normal calcium medium*). After the disruption of the junctional complex by prolonged Ca^{2+} starvation ZO-1, ZO-2 and claudin-1 were found mainly in the cytoplasm (Fig. 3.13A, *low calcium medium*). Significantly, the addition of Gö6976 (5 µM) into low calcium medium resulted in the partial translocation of all three tight junction proteins to the

A

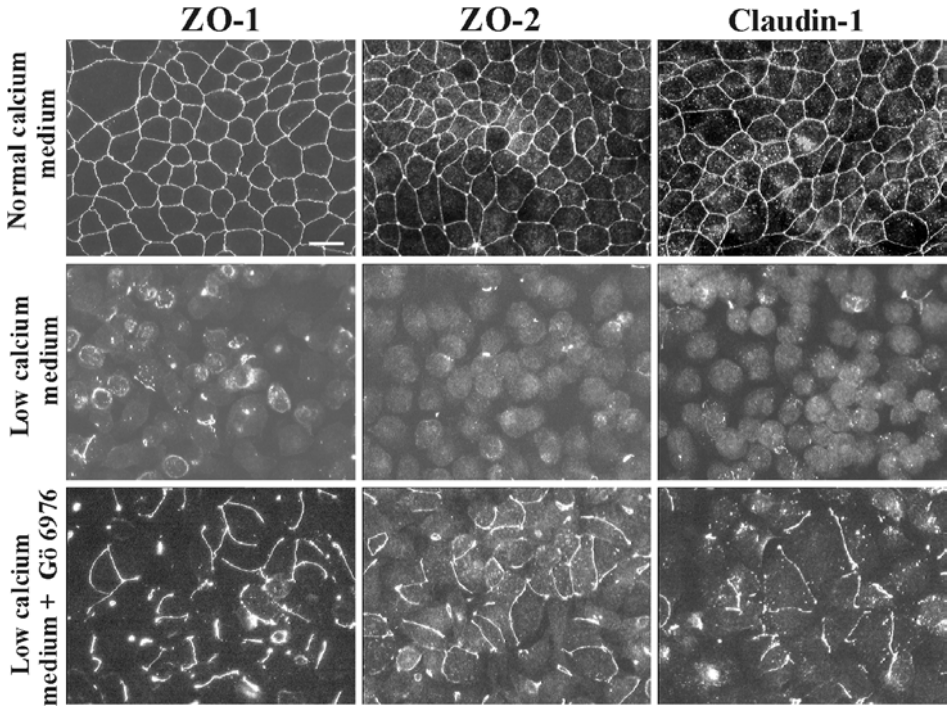

B

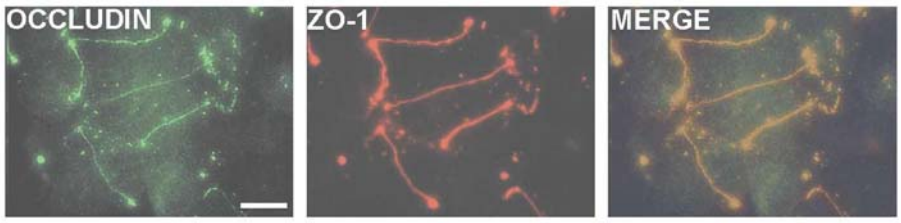

Figure 3.13 Gö6976 added to MDCK cells in low calcium medium causes relocation of ZO-1, ZO-2 and claudin-1 to intercellular contacts. Panel A, immunofluorescence localisation of ZO-1, ZO-2 and claudin-1 in MDCK cells. All proteins show characteristic staining at intercellular contacts in normal calcium medium, and diffuse cytoplasmic staining after overnight incubation in low calcium medium. Two hours after the treatment of cells incubated in low calcium medium with 5 µM Gö6976 all proteins relocate to the sites of intercellular contact. Scale bar, 20 µm.
Panel B, MDCK cells placed in low calcium medium were incubated with 5 µM of Gö6976 for 2 h. Double immunostaining of occludin and ZO-1 reveals complete colocalisation at cell-cell contacts. Scale bar, 10 µm

plasma membrane at the regions of cell-cell contact (Fig. 3.12A, *low calcium medium+ Gö6976*). Furthermore, Figure 3.13B shows that occludin and cytoplasmic tight junction protein ZO-1 co-localise at cell-cell contact sites. No cytoplasmic staining of ZO-1 is evident, although occludin shows some diffuse staining in cytoplasm. These data strongly support an assumption that Gö6976 promotes the assembly of tight junctions, that is, the inhibition of conventional PKC isozymes promotes TJ assembly under LC conditions.

3.5. Gö6976 delays tight junction disassembly induced by switch from NC to LC medium.

The disassembly of tight junctions triggered by switch to LC medium can be blocked by GF-109203X (Avila-Flores et al., 2001) suggesting the involvement of PKC. Since our data indicated that cPKC antagonises the stability of tight junction, we hypothesized that the prevention of TJ disassembly by GF-109203X is due to the inhibition of conventional PKC. To check whether cPKC are involved in the disassembly of TJs, MDCK cells were switched from NC to LC medium in the presence and in the absence of Gö6976.

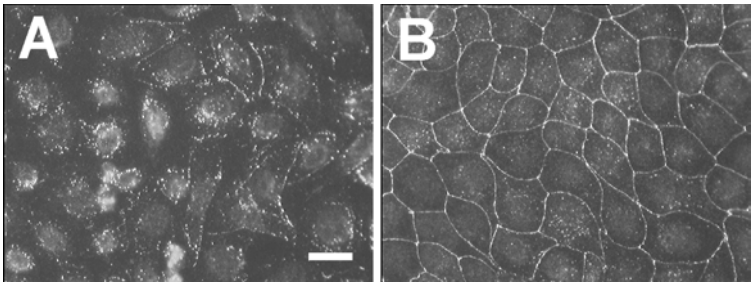

Figure 3.14 Gö6976 prevents the tight junction decomposition induced by the switch from normal to a low calcium medium. Immunostaining of occludin in MDCK cells 30 min after switch from normal to a low calcium medium (A). Occludin signal is detected mainly from cytoplasm with occasional staining at intercellular contacts indicating the decomposition of tight junctions. The relocation of occludin from tight junction to cytoplasm is blocked by 5 μM Gö6976 (B). Scale bar, 20 μm

Thirty minutes after switching to LC medium tight junctions were significantly disrupted as judged from predominantly cytoplasmic staining of occludin. When the switch to LC conditions was performed in the presence of Gö6976 (5 μM) the redistribution of occludin from tight junction to cytoplasm was completely inhibited (Fig. 3.14, A and B). In some cells treated with Gö6976 occludin was evident in relatively large granular structures located in cytoplasm (Fig. 3.14, B).

3.6. Occludin as a Substrate of PKC.

3.6.1 Expression and purification of C-terminal part of occludin.

Since our data indicated that among all PKC isoforms PKCδ is most likely to phosphorylate occludin (see Part 3.2.3), we questioned whether purified PKCδ can phosphorylate occludin *in vitro*. A cDNA encoding for cytoplasmic C-terminal tail of occludin

has been obtained by reverse transcription using total RNA from mouse kidney, random hexamer primers and MuMLV reverse transcriptase. A 777-base pair fragment encoding for amino acids 264-521 of mouse occludin has been amplified by polymerase chain reaction using Taq polymerase, reversely transcribed RNA, and occludin-specific primers (Fig. 3.15) and cloned into pCRScript vector directly from PCR reaction. A cDNA of occludin has been subcloned into pGEX-4T-1 vector to produce a construct for the expression of COOH-terminal domain of occludin fused with glutathione transferase (GST-occludin).

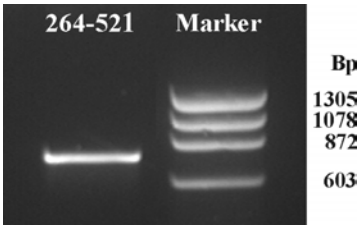

Fig. 3.15. COOH-terminal part of occludin (amino acids 264-521) obtained by RT-PCR. Ten µl of PCR reaction were resolved in agarose gel. Nucleic acids were stained with ethidium bromide.

The fusion protein was overexpressed in *E.coli* and isolated by means of affinity chromatography over glutathione column. GST-occludin was further purified by anion-exchanged chromatography and used for in vitro phosphorylation.

3.6.2 In vitro phosphorylation of occludin by PKCδ.

To investigate whether occludin may serve as a substrate for protein kinase Cδ, recombinant GST-occludin was incubated in vitro with purified PKCδ in the presence of [γ-^{32}P]ATP. As shown in Figure 3.16 an autoradiography signal was detected corresponding to a protein of approximately 60 kDa (the predicted molecular weight of GST-occludin is 59 kDa), implying that GST-occludin was phosphorylated by PKCδ. No autoradiography signal at this position was detected when GST-occludin or PKC were omitted (*GST-occludin alone, PKCδ alone*), excluding the possibilities that the autoradiography signal was due to autophosphorylation of PKC or any kinase activity which might have co-purified with GST-occludin.

A control GST protein, with a predicted molecular weight of 28 kDa was not phosphorylated (*GST+PKCδ*) indicating the relative specificity of occludin phosphorylation by PKCδ. A strong autoradiography signal at the position corresponding to the molecular weight of PKCδ was detected, indicating that PKCδ undergoes autophosphorylation. The absence of the signal in the control sample in which PKCδ has been omitted supports this assumption.

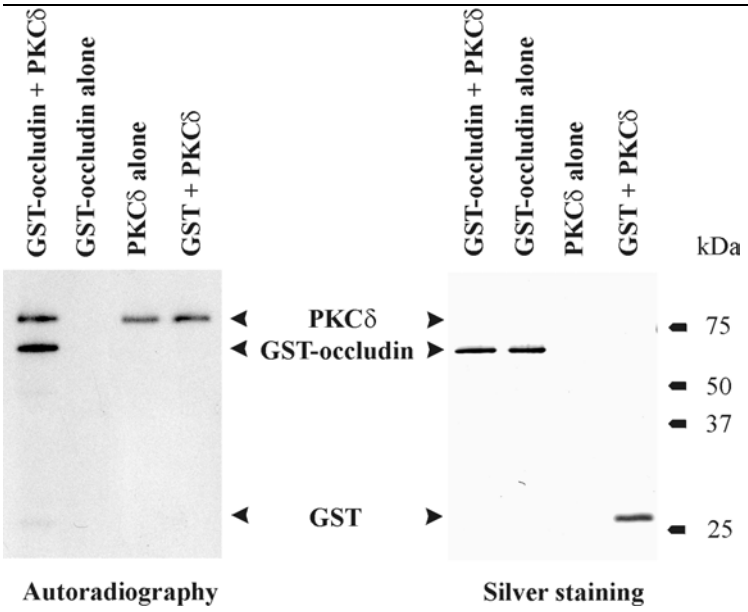

Figure 3.16 PKCδ phosphorylates the COOH-terminal domain of recombinant occludin. GST-occludin was incubated with PKCδ in a buffer containing [γ-^{32}P]ATP followed by SDS-PAGE, transfer onto nitrocellulose membrane, silver staining and autoradiography. An autoradiography signal was visible at about 60 kDa, indicating that GST-occludin is phosphorylated by PKC. No signal at this position was detected in control samples from which occludin or PKC were omitted. A strong signal at 77.5 kDa was detected, indicating that PKCδ undergoes autophosphorylation. The control protein GST was not phosphorylated.

3.7. Identification of the in vivo occludin phosphorylation sites.

3.7.1 Purification of occludin from rat liver.

Although PKCδ is capable of phosphorylation of occludin, we failed to identify phosphorylation sites using mass-spectrometric approaches. Therefore, we tried to isolate phosphorylated occludin from natural source (rat liver) for the subsequent identification of in vivo phosphorylation sites by mass-spectrometry. In MDCK cells highly phosphorylated occludin molecules are known to resist extraction with non-ionic detergent (Sakakibara et al., 1997; Wong, 1997). Hence, as an initial step to characterise biochemical properties of occludin from rat liver its solubility in TX-100-containing buffer has been analysed. Rat liver samples were cut in small pieces, homogenised in the presence of 1% TX-100 and centrifuged, the supernatant being referred to as the TX-100-soluble fraction. The pellet was further solubilised with a buffer containing 1% SDS and the supernatant obtained after centrifugation was then used as the TX-100-insoluble fraction. Both fractions were electrophoresed and immunoblotted with anti-occludin pAb. As expected, the predominant low molecular weight bands of occludin corresponding to non- or low-phosphorylated forms were mainly extracted with TX-100 (Fig. 3.17, *S*), while occludin bands with apparently higher molecular weight (highly phosphorylated forms) were selectively recovered in the TX-100 insoluble fraction (Fig. 3.17, *I*). It is important to note that the high molecular weight forms of occludin represent a minor fraction of total occludin; since the amount of occludin in TX-100 soluble fraction was considerably higher, this fraction was diluted ten times prior to the electrophoretic separation.

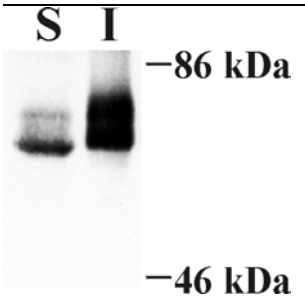

Fig. 3.17 Multiple banding pattern and detergent solubility of occludin. Immunoblot of the TX-100-soluble (S, ten times diluted) and TX-100-insoluble (I) occludin fractions with anti-occludin mAb is shown. High molecular weight forms of occludin are selectively recovered in the TX-100-insoluble fraction.

We used the property of highly phosphorylated occludin to resist TritonX-100 extraction to separate the minor phosphorylated from the major less-phosphorylated occludin forms (see Fig. 3.18 and Fig. 3.19). To this end, 50 g of rat liver were homogenised in TX-100 containing buffer (Fig. 3.18, *Total*) to aid the complete cell lysis. To remove cytoplasmic proteins and non-phosphorylated occludin forms, liver homogenate was centrifuged, the supernatant (Fig. 3.18, *1%TX)* was aspirated and the pellet has been used as a source of phosphorylated occludin. Occludin was extracted from the pellet with SDS-containing buffer and separated from SDS-insoluble cell debris by an additional centrifugation step (Fig. 3.18, *1% SDS*).

Precipitation of proteins with ammonium sulphate has been used to obtain occludin-enriched fraction from SDS-extract. For this purpose we performed repeated procedure of addition of the defined quantity of ammonium sulphate with the subsequent separation of precipitated material by centrifugation. The presence of occludin in precipitates was monitored by the immunoblot analysis of pellets and supernatants. As shown on Fig. 3.18, occludin was not precipitated with 7% or 11% of ammonium sulphate (P_7, P_{11}) but was significantly precipitated with 14% (P_{14}). This 14% ammonium sulphate precipitate, which is further referred to as phospho-occludin enriched fraction, was solubilised and used for further purification.

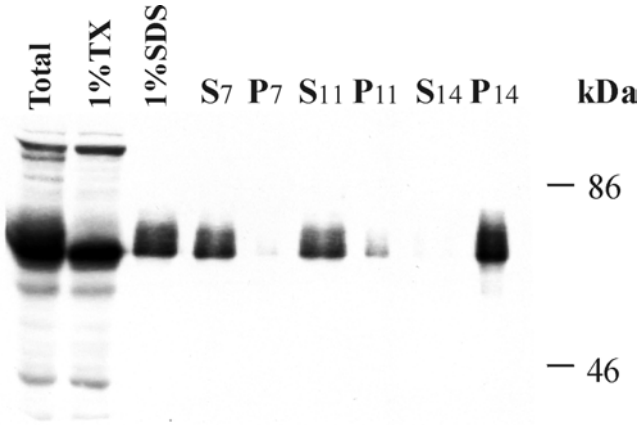

Figure 3.18 Occludin fractionation by sequential ammonium sulphate precipitation. Western blot analysis of the total homogenate of rat liver (Total), Triton X-100-soluble fraction (1% TX), SDS extract (1% SDS), supernatants (S_7, S_{11}, S_{14}) and precipitates (P_7, P_{11}, P_{14}) corresponding to the sequential 7%, 11% and 14% ammonium sulphate precipitation steps. Occludin is quantitatively recovered in the precipitate obtained with 14% ammonium sulphate (P_{14}).

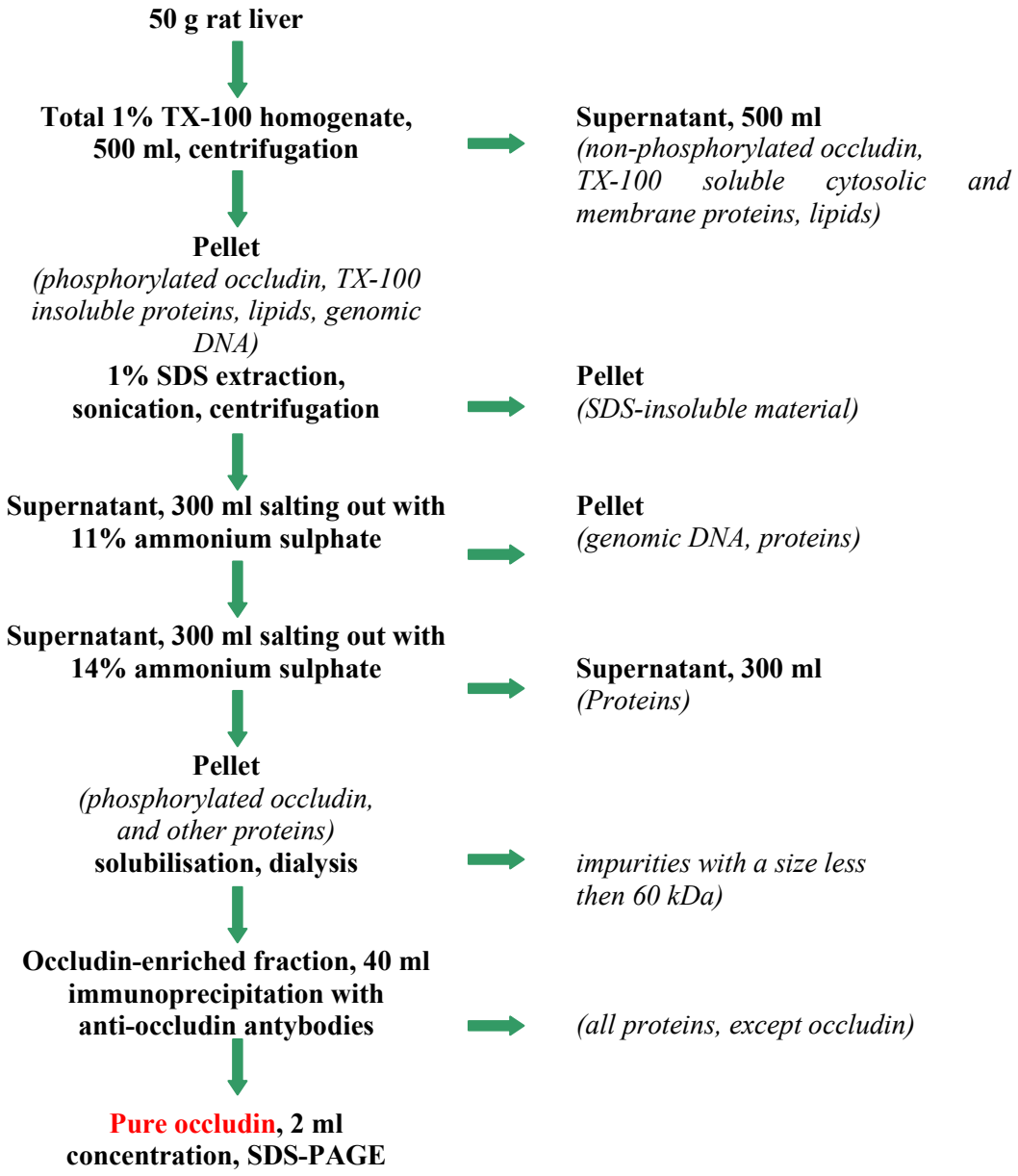

Fig. 3.19 Schematic presentation of procedure for occludin isolation from rat liver

To remove low molecular weight substances which may impede the binding of antibody to its antigen, the phospho-occludin-enriched fraction was dialysed against the Immunoprecipitation buffer. Occludin was immunoprecipitated with polyclonal anti-occludin antibodies covalently bound to Protein A gel (see Materials and Methods). The analysis of the efficiency of immunoprecipitation (Fig. 3.20) revealed that occludin was quantitatively and selectively recovered in fractions eluted with a low pH buffer. This purified occludin was concentrated on the diatomaceous earth, resolved by SDS-PAGE and stained with colloidal

Coomassie blue. We observed single, significantly smeared band at about 63 kDa which corresponds to the predicted molecular weight of occludin.

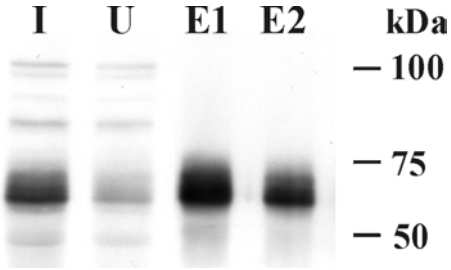

Fig. 3.20 The immunoprecipitation of occludin from occludin-enriched fraction. Immunoblot analysis with anti-occludin pAb.
I–initial phospho-occludin-enriched fraction dialysed overnight against immunoprecipitation buffer. U–unbound material. E1, E2–fractions obtained from sequential elution with a low pH buffer.

3.7.2 Mass spectrometric identification of occludin-derived peptides.

In order to confirm the identity of occludin in isolated sample we used MS peptide mapping strategy. A band corresponding to approximately 63 kDa was cut off Coomassie-stained gel, subjected to proteolytic in-gel digestion with Asp-N endopeptidase followed by the extraction of peptides and mass-spectrometric analysis by MALDI MS (Fig. 3.21 Panel A). The obtained MALDI MS data were analysed by means of Internet program (MS-Fit). This algorithm compares a set of detected peptide masses generated by enzymatic digestion of protein with theoretical peptide masses calculated from each sequence entry in the database using the same cleavage specificity as the reagent in the experiment. A search in two databases Ludwignr. and NCBInr. identified *Rattus norvegicus* (rat) occludin as the only protein present in the sample (accession numbers 13786154 and AB016425 in NCBInr. and Ludwignr., respectively), confirming that the purification was successful. Nevertheless, many observed peptide masses did not match predicted occludin peptide masses, suggesting the presence of trace amounts of contaminating proteins. The experimentally obtained masses which matched theoretical masses of occludin peptides are listed in Table 3.1.

Obviously, the peptides detected by MS cover only a small portion (about 10%) of occludin sequence, probably due to reduced solubility, ionisation and desorption properties of some occludin-derived peptides. To overcome the problem of incomplete coverage of the protein a parallel digest of occludin band with an enzyme of differing specificity, namely trypsin, has been performed. Masses of tryptic peptides were determined by MALDI MS and analysed using on-line Internet FindMod program, which correlates observed masses with a set of theoretical peptide masses for amino acid sequence of protein of interest. Analysis of tryptic peptides further

ascertained the identity of occludin to the isolated protein and assigned additional matching regions within the occludin sequence. Matched tryptic peptides are shown in Table 3.2.

Table 3.1. The results of MS-Fit search using mass data generated by MALDI MS analysis of protein band digested with Asp-N.

m/z submitted	MH^+ matched	Mass Difference, Da	#MC	Database Peptide Sequence	Position, amino acid Nr.
942.415	942.4679	0.0529	0	ESPPPYRP	7-14
1418.561	1418.6335	0.072	0	DEFKPNHYAPSN	15-26
1302.558	1302.5823	0.024	0	DQYLYHYCVV	230-239
804.326	804.3886	0.063	0	DKEHIY	282-287
752.299	752.3573	0.058	0	DYAERV	314-319
1384.569	1384.6240	0.055	1	DDFRQPRYSSN	362-372
1269.533	1269.5971	0.064	0	DFRQPRYSSN	363-372
1495.701	1495.7764	0.075	0	DQQRQLYKRNF	427-437
1507.721	1507.7863	0.065	0	DEYNRLKQVKGSA	480-492

Table 3.2. The results of FindMod search based on mass data obtained by MALDI MS analysis of occludin band digested with trypsin

m/z submitted	MH^+ matched	Mass Difference, Da	#MC	Peptide Sequence	Position, amino acid Nr.
1012.562	1012.5574	-0.004	0	WTSPPGVIR	58-66
2031.895	2031.9076	0.013	0	NVSAGTQDMPPPPSDYAER	300-318
2422.258	2422.2863	0.028	0	SPPLVPEVAQEIPLTLSVDDFR	344-365
2803.483	2803.4988	0.016	1	SPPLVPEVAQEIPLTLSVDDFRQPR	344-368
1510.690	1510.7132	0.023	1	YSSNDNLETPSKR	369-381
1333.641	1333.6382	-0.002	0	EYPPITSDQQR	420-430
1340.644	1340.6593	0.015	1	RNFDAGLQEYK	435-445
1184.556	1184.5582	0.002	0	NFDAGLQEYK	436-445
1715.897	1715.9173	0.02	1	SLLAELDEVNKELSR	446-460
2100.102	2100.1295	0.028	2	SLLAELDEVNKELSRLDR	446-463

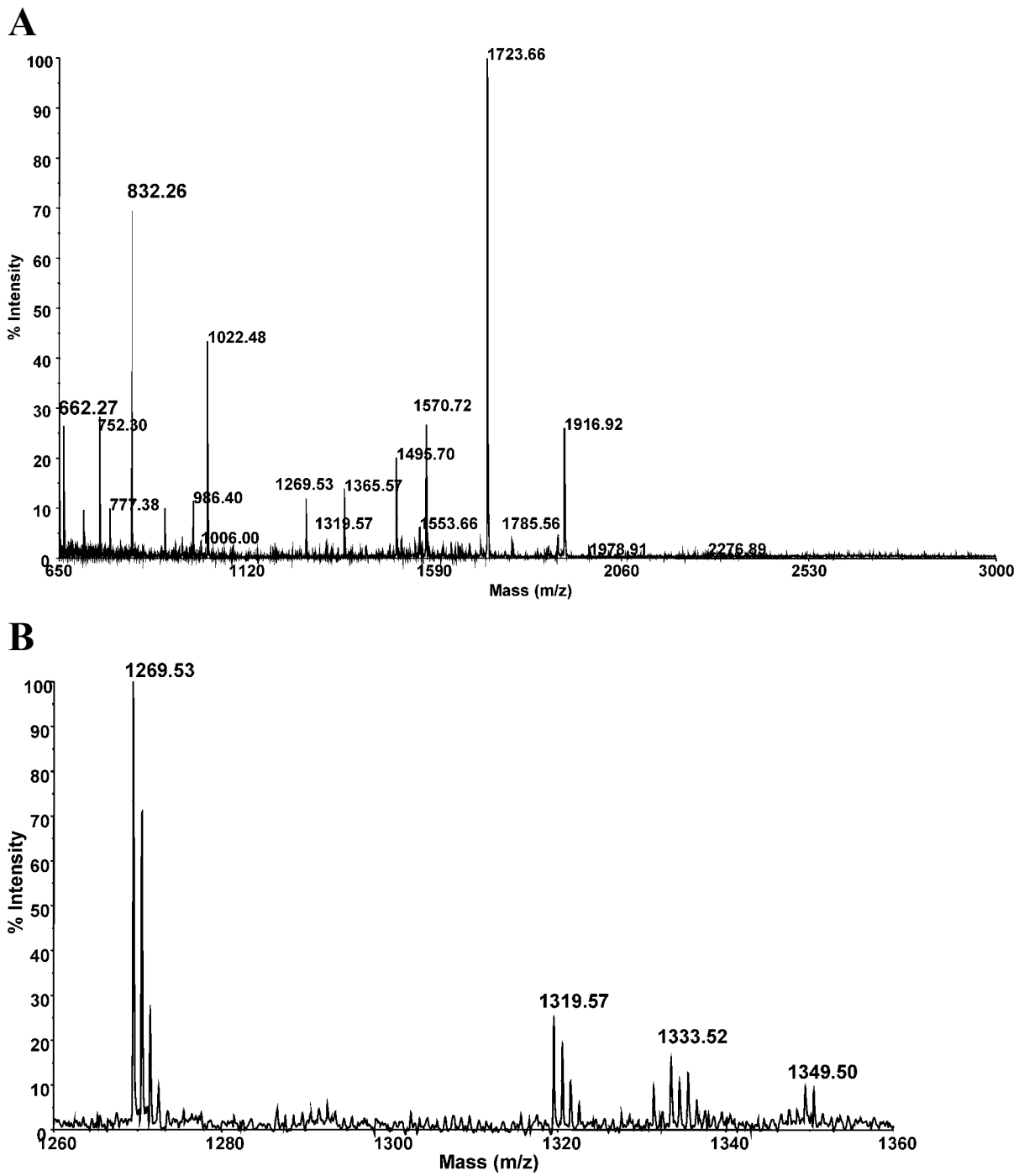

Fig. 3.21. Peptide mass fingerprint analysis of the immunoprecipitated protein. Protein was in-gel digested with Asp-N, the peptides were extracted, purified over C18 reversed-phase minicolumn, mixed with an α–cyano-4-hydroxycinnamic acid matrix and analysed by MALDI-TOF-MS. *Panel A* shows MALDI mass spectra recorded in the reflection mode. The peaks with m/z 662.27 and 832.26 correspond to the phosphorylated sequences ^{467}DYRE and ^{314}DYAERV, respectively. *Panel B*: An expansion of the region of upper mass spectrum reveals satellite peaks that arise owing to the isotopic composition of the peptide. Within each isotopically resolved ion cluster the first most intensive peak represents the peptide with monoisotopic mass. The peaks with m/z 1269.53 and 1349.50 correspond to the non-phosphorylated and phosphorylated sequense ^{263}DFRQPRYSSN, respectively.

On the next step mass-spectrometrical data were analysed for the presence of phosphorylated peptides since it is well known that if experimental mass determined by MALDI-TOF MS exceeds the theoretical monoisotopic mass on 79.9663 Da (corresponds to PO_3-), it points on the potential phosphorylation of the peptide. To verify if any of peaks registered by MALDI MS correspond to the phosphorylated fragment of occludin we screened by means of ExPASy FindMod program all experimentally detected mass peaks obtained with trypsin and Asp-N, searching for mass differences consistent with phosphorylation (i.e. +80 Da). The outcomes of the FindMod quests are summarised in Table 3.3. The search revealed that three peaks registered by MALDI MS analysis of the peptide mixture, obtained by occludin digestion with Asp-N correspond to potentially phosphorylated occludin peptides (Fig. 3.21). Assuming that only Ser, Thr and Tyr residues are phosphorylated, we analysed the amino acid sequences of these peptides for potential phosphorylated residues. The peptides with m/z 662.27 and 832.26 corresponding to the phosphorylated sequences ^{467}DYRE and ^{314}DYAERV, respectively, contain only one amino acid residue (Tyr) which could be phosphorylated, allowing unambiguous assignment of the potentially phosphorylated sites. The peptide of m/z 1349.50 corresponding to the ^{263}DFRQPRYSSN contains one Tyr and two Ser, complicating the prediction of phosphorylated site. The search on the MALDI MS data obtained from samples digested with trypsin did not reveal any potential phosphorylation.

However, the MALDI MS analysis of peptide mixtures only assigns peptides which may be phosphorylated, neither proving that the detected mass corresponds to the given phosphorylated peptide nor giving the information on the exact amino acid residue which is phosphorylated. The detected ions may be in fact some non-phosphorylated peptides, derived by non-specific proteolysis or cleavage by contaminating protease. To prove that the observed mass peak indeed corresponds to the peptide of interest and to identify the exact site of phosphorylation the sequencing with tandem mass-spectrometry (MS/MS) must be performed.

Table 3.3. Potentially phosphorylated peptides detected by mass difference using FindMod search programm.

Mass Submitted, Da	Database Mass, Da	Mass Difference, Da	modif. difference, Da	Δ mass, Da	#MC	Peptide Sequence	Position, amino acid Nr.
832.262	752.3573	79.9047	79.9663	0.062	0	DYAERV	314-319
1349.505	1269.5971	79.9079	79.9663	0.058	0	DFRQPRYSSN	363-372
662.269	582.2518	80.0172	79.9663	-0.05	1	DYRE	467-470

3.7.3 Sequencing of the occludin derived peptides by LC-MS/MS.

To confirm that mass peaks with m/z 1269.5971, 752.3573 and 662.2181, identified by MALDI MS, represent phosphorylated occludin peptides and to identify the phosphorylated residues we subjected occludin sample digested with Asp-N for MS/MS analysis. Unfortunately, the ions with m/z corresponding to the peptides of interest were not detected among those transmitted through the first quadrupole analyser of nanoelectrospray mass spectrometer, making the subsequent selection, fragmentation and sequencing impossible. Since, occludin samples subjected to the MALDI or ESI MS analysis were identical (originating from the same preparation), it is unlikely that these peptides were absent in the probe. Therefore, we concluded that peptides with m/z 1269.5971, 752.3573 and 662.2181 failed to be desorbed or ionised by ESI approach. To overcome this problem a parallel digest of occludin with trypsin has been performed. Trypsin cleavage specificity differs from that of Asp-N resulting in peptides with another amino acid composition and, hence, another ionisation properties. We selected only those tryptic peptides for the sequencing analysis, which contained predicted phosphorylated residues. Thus, peptide DFRQPR**YSS**N (363-372) obtained by Asp-N cleavage contains three residues which may be phosphorylated: two Ser and one Tyr residue. Accordingly, tryptic peptide **YSS**NDNLETPSK (369-380) which contains these presumably phosphorylated residues was selected for the sequencing analysis. Similarly, remaining two tryptic peptides NVSAGTQDMPPPPSD**Y**AER and ELDD**Y**R were selected for sequencing analysis by MS/MS instead of D**Y**AERV and D**Y**RE (Table 3.4). The predicted m/z values of occludin tryptic peptides containing putatively phosphorylated residues are summarised in Table 3.4.

Table 3.4. Theoretical monoisotopic masses of occludin tryptic peptides.

Tryptic peptides	Position, amino acid Nr.	m/z of peptide $[M+H]^+$	m/z of phosphory-lated peptide $[M+H]^+$	m/z of doubly charged phosphorylated peptide $[M+2H]^{2+}$
NVSAGTQDMPPP PSDYAER	300-318	2031.9076	2111.8739	1056.4409
YSSNDNLETPSK	369-380	1354.6121	1434.5784	717.7931
ELDDYR	464-469	810.3628	890.3291	445.6685

Parent ion scan revealed two doubly charged mass peaks corresponding to both phosphorylated and non-phosphorylated ^{369}**YSS**NDNLETPSK peptides (Fig. 3.22A, peaks 717.79 and 677.81). They were both isolated from parent ion mixture in the first quadrupole of mass spectrometer, decomposed with argon in a quadrupole collision cell and the masses of resulting fragmented ions were determined by TOF analysis. The collision-induced

decomposition (CID) spectra of both parent ions are presented on Fig. 3.22A and B. These spectra confirm the sequence of the peptide and allow the identification of the site of phosphorylation as Ser 371.

A

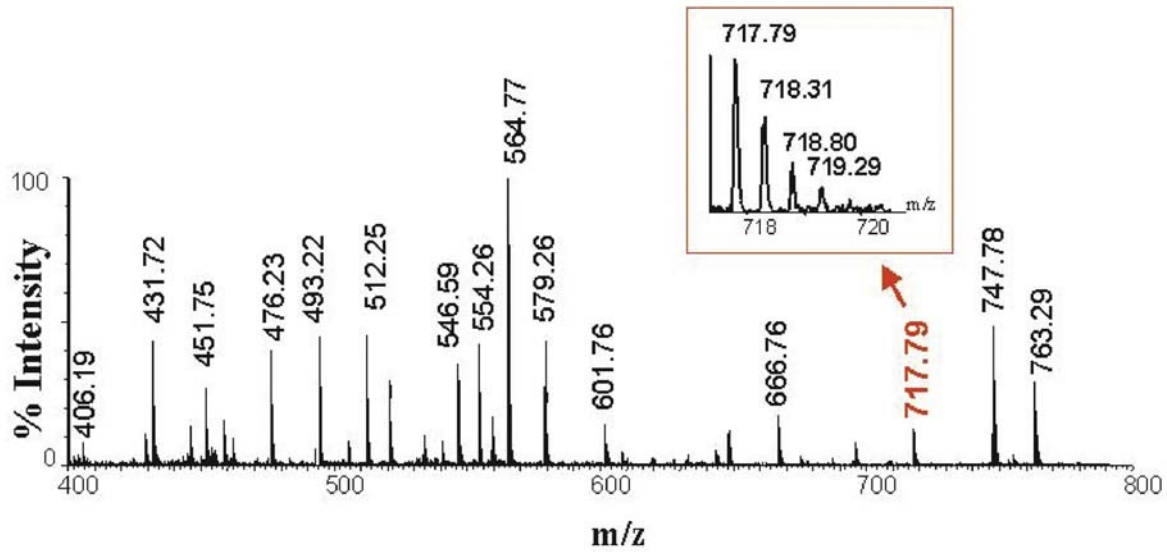

B

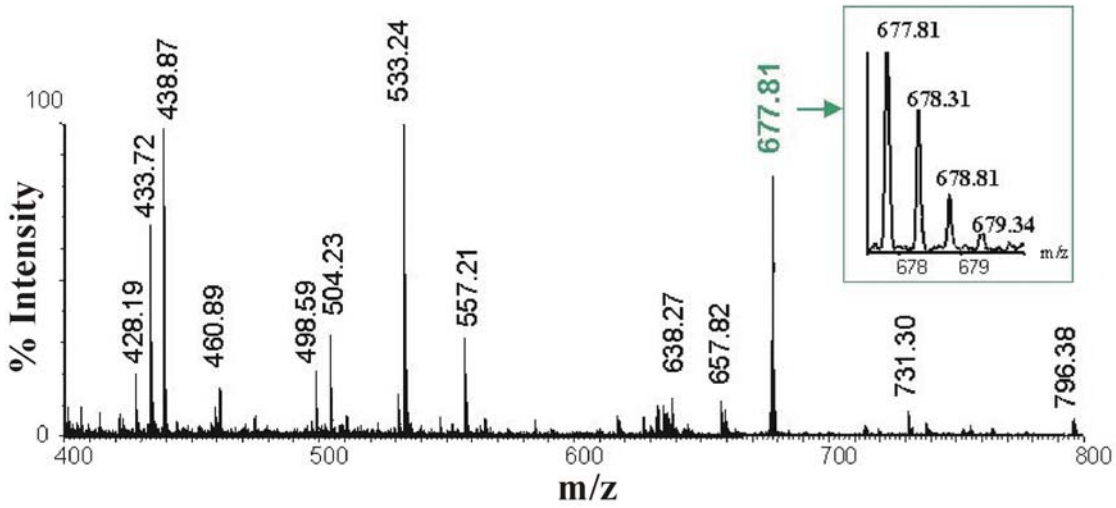

Fig.3.22 Nanoelectrospray analysis of a fraction from the tryptic digest of 63 kDa protein. The protein was purified by SDS-PAGE, digested with trypsin, and the peptides analysed by LC-ESI-MS. Nanoelectrospray mass spectra from two MS measurements are shown. Panel A: A peak with m/z 717.79 corresponding to phosphorylated peptide YSSNDNLETPSK is visible. Panel B: A peak with m/z 677.81 corresponding to peptide YSSNDNLETPSK without postranslational modifications is evident. The insets represent the peaks of interest at higher resolution. Expansion reveals the presence of at least four isotopic variants of each peptide.

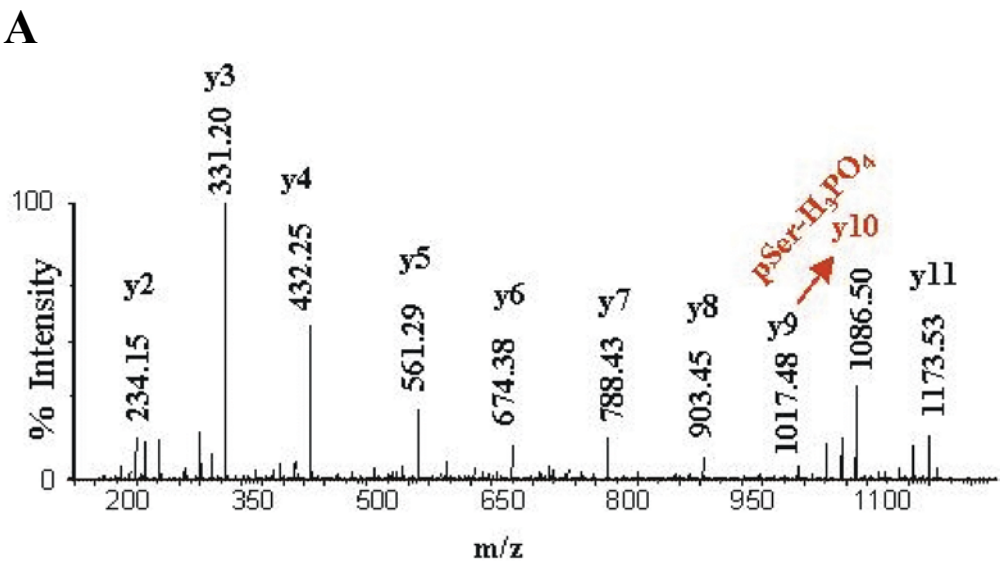

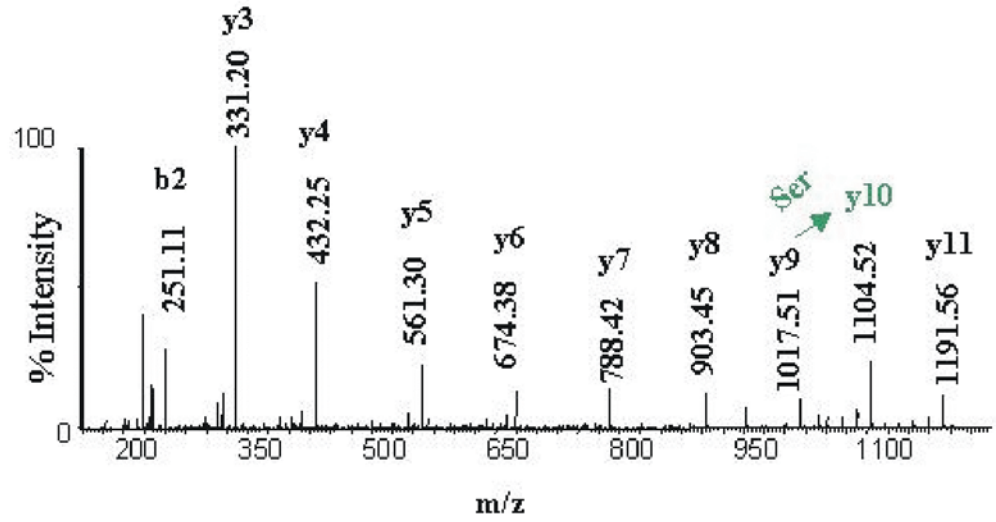

C

	12	11	10	9	8	7	6	5	4	3	2	1	y
	Y	S	S	N	D	N	L	E	T	P	S	K	
b	1	2	3	4	5	6	7	8	9	10	11	12	

Fig. 3.23. Mapping of the phosphorylation site in occludin using a tryptic digest mixture. Collision-induced decomposition spectra of the doubly charged ions corresponding to ^{369}YSSNDNLETPSK peptide. The spectra confirm the sequence of the peptide and identify the site of phosphorylation as Ser371. *Panel A*: the tandem mass spectrum of phosphorylated peptide $(M+2H)^{2+}/z$ 717.79. The difference between the masses of y9 and y10 corresponds to pSer-H_3PO_4 (Ser-H_20), indicating the loss of H_3PO_4. The y10 signal 1104.52, confirming the addition of entire Ser was not detected *Panel B*: the tandem mass spectrum of non-phosphorylated $(M+2H)^{2+}/z$ 677.81 is shown, identifying the strong signal for y10 (y9+Ser) 1017.49+87.03=1104.52 without loss of H_2O. Relevant ions are labelled according to the accepted nomenclature (*Panel C*).

The deduction of phosphorylation site comes from the m/z differences between fragmented ions. The phosphoserine, phosphothreonine and phosphotyrosine undergo facile preferential loss of H_3PO_4 (Δ= - 98 Da) during CID (Qin and Chait, 1997). Hence, the mass difference between peptide fragment containing previously phosphorylated residue (y_{n+1}) and peptide where this residue was removed (y_n) by CID would be mass of phospho-Ser/Thr/Tyr – mass H_3PO_4 (or Ser/Thr/Tyr – mass H_2O). In the absence of phosphorylation the mass difference would be equal to pure Ser/Thr/Tyr mass.

Since in our experiment we observed the difference in the masses between y_{n+1} and y_n corresponding to the phospho-Ser/Thr/Tyr – mass H_3PO_4 only for NDNLETPSK (y9) and **S**NDNLETPSK (y10), we conclude that Ser 371 is phosphorylated.

Unfortunately, the peaks with m/z values corresponding to the two putatively phosphorylated tryptic peptides ^{300}NVSAGTQDMPPPPSD**Y**AER and ^{464}ELDD**Y**R were not detected in ESI-MS. Thus, phosphorylation of Tyr315 and Tyr468 remains to be confirmed.